

# The use of the first and of the second order phase magnetic transition alloys for an AMR refrigerator at room temperature: A numerical analysis of the energy performances

C. Aprea<sup>a</sup>, A. Greco<sup>b,\*</sup>, A. Maiorino<sup>a</sup>

<sup>a</sup> Dipartimento di Ingegneria Meccanica, Università di Salerno, via Ponte Don Melillo, 84084 Fisciano, Salerno, Italy

<sup>b</sup> DETEC, Università degli Studi di Napoli Federico II, P.le Tecchio 80, 80125 Napoli, Italy

## ARTICLE INFO

### Article history:

Received 12 November 2012

Accepted 19 February 2013

### Keywords:

AMR

Magnetic materials

First order phase transition

Second order phase transition

Gd

Gd<sub>x</sub>Dy<sub>1-x</sub>

Gd<sub>x</sub>Tb<sub>1-x</sub>

Gd<sub>5</sub>(Si<sub>x</sub>Ge<sub>1-x</sub>)<sub>4</sub>

MnAs<sub>1-x</sub>Sb<sub>x</sub>

## ABSTRACT

The magnetic refrigeration is a new highly efficient and environmentally protective technology, which could be an actual solution for the typical problems of the vapour compression systems. The core of a magnetic refrigerator system is the Active Magnetic Regenerator (AMR). It is a special kind of thermal regenerator made of magnetic material which works both as a refrigerating medium and as a heat regenerating medium. The performance of an AMR system strongly depends on the magnetocaloric effect of the magnetic material used to build the regenerator.

In the present paper, a model to simulate the thermal behaviour of an AMR has been introduced for predicting the performance of an AMR refrigerator system. Different magnetic materials have been considered as refrigerant: pure gadolinium, second order phase magnetic transition binary rare earth alloys (SOMT) and first order phase magnetic transition alloys (FOMT). The SOMT are Gd<sub>x</sub>Dy<sub>1-x</sub> and Gd<sub>x</sub>Tb<sub>1-x</sub> whereas the FOMT are Gd<sub>5</sub>(Si<sub>x</sub>Ge<sub>1-x</sub>)<sub>4</sub> and MnAs<sub>1-x</sub>Sb<sub>x</sub>. The magnetocaloric behaviour of gadolinium can be correctly predicted by the Weiss molecular field theory. This approach can be generalized for binary alloys with a second order phase transition. The behaviour of the MnAs<sub>1-x</sub>Sb<sub>x</sub> alloys is described by means of a model based on the phenomenological approach of Bean Rodbell. Interpolation of empirical data is utilized for the evaluation of the magnetocaloric effect of Gd<sub>5</sub>(Si<sub>x</sub>Ge<sub>1-x</sub>)<sub>4</sub> alloys.

With this model, the refrigeration capacity, the power consumption and consequently the Coefficient of Performance of the cycle can be predicted. The results of the simulation clearly show that Gd<sub>5</sub>(Si<sub>x</sub>Ge<sub>1-x</sub>)<sub>4</sub> is the best magnetic material with a COP that is always greater than that of a traditional vapour compression plant in the same operating conditions (from a minimum of +40% to a maximum of +62%).

© 2013 Elsevier Ltd. All rights reserved.

## 1. Introduction

Modern refrigeration is almost entirely based on vapour compression plant. This is a mature, reliable and low cost technology [1–4]. The refrigerant fluids used contribute to the ozone layer depletion and to the global warming. Although the Montreal Protocol has restricted the harm to the environment of ODS (Ozone Depletion Substances), the greenhouse effect problem is not solved yet [5,6].

Magnetic refrigeration is an emerging and an environmental friendly technology. It is based on the magneto-caloric effect in solid-state refrigerants (MCE) [7,8] and has the potential for achieving higher energetic efficiencies than the traditional vapour compression ones. The high efficiency arises because the analogues to the compression and expansion parts of the vapour compression

cycle are accomplished by the magnetization and demagnetization of a magnetic material and therefore there is a reduction in the irreversibilities of the whole plant. This technology does not have ozone-depleting and greenhouse effects. Indeed, the magnetic refrigerant is a solid and has essentially zero vapour pressure and therefore is ecologically sound.

A larger MCE in refrigerant material results in a greater change of internal energy and provides more cooling that needs to be transferred out of the bed by the exchange fluid. The MCE originates from coupling a magnetic field with magnetic moments carried by itinerant or localized electrons. At the Curie temperature a magnetic material exhibits its maximum MCE. There are two types of magnetic phase changes that may occur at the Curie point: first order magnetic transition (FOMT) and second order magnetic transition (SOMT). A FOMT exhibits a discontinuity in the first derivative of the Gibbs free energy, whereas a SOMT is continuous in the first derivative but exhibits discontinuity in a second derivative of the free energy. Therefore in a FOMT the magnetization, which is the first derivative of the free energy with the applied magnetic

\* Corresponding author. Tel.: +39 0817682289; fax: +39 0812390364.

E-mail address: [adriana.greco@unina.it](mailto:adriana.greco@unina.it) (A. Greco).

**Nomenclature***Symbols*

$A$	heat transfer surface, m <sup>2</sup>
$B$	magnetic induction, T
$B_j$	Brillouin function
$C$	specific heat, J/kg K
COP	Coefficient of Performance
$D$	diameter of the regenerator section, m
$d_p$	diameter of the particles, m
$g_j$	Landè factor
$h$	heat transfer coefficient, W/m <sup>2</sup> K
$H$	magnetic field strength, A/m
$J$	total angular momentum quantum
$K$	Boltzman constant, J/K
$k$	thermal conductivity, W/m K
$K$	compressibility coefficient
$K_{eff}$	effective thermal conductivity, W/m K
$L$	length of the regenerator, m
$M$	magnetization, A/m
$M_m$	molar mass, kg/mol
$m$	mass, kg
$N$	number of atoms per volume, 1/m <sup>3</sup>
$Na$	number of atoms per molecule
$p$	pressure, Pa
$Pr$	Prandtl number
$Q$	thermal energy, J
$R$	universal constant gas, J/mol K
$S$	entropy, J/K
$s$	specific entropy, J/kg K
$T$	temperature, K
$t$	time, s
$v$	specific volume, m <sup>3</sup> /kg
$W$	work, J
$w$	local velocity, m/s
$x$	space, m
$x$	mass fraction

*Greek symbols*

$\beta$	slope of $T_c$ curve on the cell deformation
$\gamma$	electronic constant, J/K mol
$\Delta$	finite difference, –

$\delta$	error, K
$\varepsilon$	porosity, –
$\eta$	isentropic efficiency, –
$\eta$	parameter of the order of the magnetic phase transition
$\mu$	viscosity, Pa s
$\mu_B$	Bohr magneton, J/T
$\mu_0$	vacuum magn. perm., T m/A
$\omega$	cell deformation

*Subscripts*

$ad$	adiabatic
$B$	magnetic field constant
$b$	bed
$C$	Curie
$c$	cold
$CF$	cold water flow
$D$	demagnetization phase
$De$	Debye
$el$	electronic
$eq$	taken at equilibrium
$f$	fluid
$h$	hot
$H$	magnetic field constant
$HF$	hot water flow
$inf$	undisturbed flow
$lat$	lattice
$M$	magnetization phase
$m$	magnetic
$max$	maxim
$MC$	Carnot machine
$o$	Curie in absence of deformation
$p$	particle
$ref$	refrigeration
$rej$	reject
$sc$	effective heat transfer
$s$	solid
$T$	constant temperature
$tot$	total
$tr$	trial

field strength, is discontinuous. In a SOMT the magnetic susceptibility, which is the second derivative of the free energy with the field, changes discontinuously. Most of the magnetic materials order with a SOMT from a paramagnet to a ferromagnet, ferrimagnet or antiferromagnet [9].

In the case of ferromagnetic materials the magnetocaloric effect (MCE) is a warming as the magnetic moments of the atom are aligned by the application of a magnetic field, and the corresponding cooling upon removal of the magnetic field. Indeed, when a magnetic field is applied the magnetic moments become aligned parallel to the magnetic field which causes an increase in the magnetic order and, consequently, a decrease in the magnetic entropy. Therefore in an adiabatic internally reversible process (consequently at constant entropy) the lattice vibrations increase causes the temperature rising for the magnetic material. Suppressing the external field, the moments lose their orientation increasing the magnetic entropy and decreasing electronic and lattice entropy. Therefore the magnetic material cools down. The MCE, in a SOMT material, can be measured in terms of the above mentioned adiabatic temperature change ( $\Delta T_{ad}$ ) or in terms of the isothermal magnetic entropy change ( $\Delta S_M$ ) upon magnetic field variations.

Considering an internally reversible process the MCE in a SOMT material can be related to the following measurable physical quantities [10]:

$$(\Delta S_M)_T = \mu_0 \int_{H_i}^{H_f} \left( \frac{\partial M}{\partial T} \right)_H dH \quad (1)$$

$$(\Delta T_{ad})_s = -\mu_0 \int_{H_i}^{H_f} \frac{T}{C_H} \left( \frac{\partial M}{\partial T} \right)_H dH \quad (2)$$

Therefore the MCE peaks when  $\left| \left( \frac{\partial M}{\partial T} \right)_H \right|$  reaches its maximum value, i.e. around the Curie temperature in a ferromagnet or near absolute zero in a paramagnet.

The FOMT materials experience a simultaneous ordering of magnetic dipoles and a latent heat associated with the transition. A first order phase transition theoretically should occur at constant temperature and therefore,  $\left| \left( \frac{\partial M}{\partial T} \right)_H \right|$  may be infinitely large, consequently giving rise to a giant magnetocaloric effect. Some FOMT materials experience a coupled magnetic and crystallographic phase transition. Therefore in this case when a magnetic field is applied to the material the magnetic state change from a paramagnet

or an antiferromagnet to a ferromagnet simultaneously with either a structural change or a substantial phase volume discontinuity but without a clear crystallographic modification.

Partial first derivatives of Gibbs free energy with the respect to  $T$  or  $H$  are discontinuous at the first order phase transition. As a result, the bulk magnetization changes by  $\Delta M$  and  $C_H$  tends to infinite at the Curie temperature. For FOMT materials, the isothermal magnetic entropy change ( $\Delta S_M$ ) can be evaluated with the following equation based on the Clausius–Clapeyron equation:

$$(\Delta S_M)_T = \left( \frac{dH}{dT_c} \right)_{eq} (\Delta M)_T \quad (3)$$

where the derivative is taken at equilibrium.

The observed giant MCE in FOMT materials is the sum of the conventional magnetic entropy-driven process (magnetic entropy change  $\Delta S_M$ ) and the difference in the entropies of the two crystallographic modifications (structural entropy change  $\Delta S_{ST}$ ). The latter contribution accounts for the larger entropy change of FOMT respect to the SOMT materials [11,12]:

$$(\Delta S)_T = (\Delta S_M)_T + (\Delta S_{ST})_T \quad (4)$$

Postulating that  $T/C_H$  is constant, the adiabatic temperature variation in a FOMT material can be approximated as follow:

$$(\Delta T_{ad})_s \cong -\mu_0 \left( \frac{T}{C_H} \right) \left( \frac{dH}{dT_c} \right) (\Delta M)_T \quad (5)$$

The adiabatic temperature variation is larger in most of the FOMT materials than that of SOMT.

The temperature change in the SOMT materials is almost instantaneous; in the FOMT materials that experience a change in structure, atoms are displaced during the change in crystal structure and therefore the time required can be many orders of magnitude larger. This could be a problem because usually the magnetic refrigerators will operate between 0.5 and 10 Hz and much of the giant MCE may not be utilized during the rapid magnetic field increase and decrease. Thus in a real working machine magnetization and demagnetization are dynamic steps, and in some cases may become non-equilibrium processes.

SOMT materials generally exhibit very low hysteresis, whereas the FOMT materials can exhibit significant hysteresis.

Another problem that arises in the use of the FOMT materials is the large volume change. Indeed, all the FOMT materials are intermetallic compounds and are brittle. Therefore most of them will undergo some fracture, the small particles of the magnetic material would clog the regenerator bed, reducing the flow of the heat transfer fluid and lowering the cooling power.

A good material for the refrigeration at room temperature is gadolinium, which is a member of the lanthanide group of elements [13–30]. At the Curie temperature  $T_c$  of 294 K, Gd undergoes a second order paramagnetic – ferromagnetic phase transition.

A variety of Gd – R alloys, where R is another lanthanide metal have been prepared in an attempt to improve the MCE in Gd. Gd can be alloyed with terbium (Tb) [31], dysprosium (Dy) [32], or erbium (Er) [33]. However, all alloying additions just shift the Curie temperature of Gd to lower temperatures without any noticeable improvement in its MCE. Using alloys it is possible to fabricate a layered bed composed of several magnetic alloys, each placed at the location in the regenerator where the average temperature is near its Curie temperature.

Alloys composed of gadolinium, silicon and germanium exhibit a magnetocaloric effect larger than that of Gd alone and have a phase transition temperature that is in the room temperature range. The Curie temperature can be adjusted by varying the fraction of silicon. Most  $Gd_5Si_{4-x}Ge_x$  compounds (where  $0 < x < 0.5$ ) are FOMT materials and the entropy change with magnetization is

larger than that of Gd, but is also much sharper, occurring over a narrower temperature range. A magnetic hysteresis has been found for these alloys, with a value of 2 K reported for  $Gd_5Si_2Ge_2$ . An extremely large MCE has been discovered in  $Gd_5Si_2Ge_2$  when subjected to a change in the magnetic field. This alloy orders ferromagnetically at the Curie temperature of 299 K and then upon further cooling it undergoes a first order phase transition from the high temperature ferromagnetic to a second ferromagnetic structure at 276 K.

The recently developed  $MnAs_{1-x}Sb_x$  (with  $0 < x < 0.4$ ) compounds are FOMT materials that may be suitable for magnetic refrigeration systems [34,35]. The Curie temperature of the alloy varies in the range of 220–318 K. The alloy  $MnAs$  has a giant MCE in the room temperature range, with a first order transition temperature of 318 K. The transition is associated with a structural transformation. However, the FOMT of  $MnAs$  is accompanied by a large thermal hysteresis, which is unfavourable for practical use. Substituting antimony (Sb) for arsenic (As), when the fraction of Sb is greater or equal to 0.05, the thermal hysteresis becomes quite small, while the magnetocaloric effect remains approximately unchanged. However, the adiabatic temperature change for these compounds is relatively low and the thermal conductivity is significantly lower than that of gadolinium and other magnetic materials.

The main objective of this paper is to investigate the effect of the different magnetic materials on the refrigeration capacity and on the efficiency of the AMR cycle. To this hope, a practical model for predicting the refrigeration capacity and the efficiency of an AMR cycle in room temperature range has been developed. Different magnetic materials have been considered as refrigerant: pure gadolinium, second order phase magnetic transition binary rare earth alloys ( $Gd_xDy_{1-x}$  and  $Gd_xTb_{1-x}$ ) and first order phase magnetic transition alloys ( $Gd_5(Si_xGe_{1-x})_4$  and  $MnAs_{1-x}Sb_x$ ). The models simulates the magnetization and demagnetization process of the magnetic material and the regenerative warm and cold blow processes. In the simulation the magnetocaloric behaviour of gadolinium can be correctly predicted by the Weiss molecular field theory. This approach can be generalized for binary alloys with a second order phase transition. The behaviour of the  $MnAs_{1-x}Sb_x$  alloys is described by means of a model based on the phenomenological approach of Bean Rodbell. Interpolation of empirical data is utilized for the evaluation of the magnetocaloric effect of  $Gd_5(Si_xGe_{1-x})_4$  alloys.

## 2. A state of the art on magnetic materials in experimental applications

In 1976, at Lewis Research Centre of American National Aeronautics and Space Administration, Brown first applied the magnetic refrigeration in room temperature range [36]. By employing gadolinium (Gd) as the magnetic working substance, he attained a 47 K no-load temperature difference in a 7 T magnetic field.

Different mechanical realizations of AMR cycles are possible and several prototype systems have been constructed. Most of the regenerators of the experimental plants are made of gadolinium. Some of these prototypes have implemented layered regenerators beds with gadolinium based alloys. Only few regenerators are made with magnetic materials with first order transition phase.

A summary of the most significant prototype systems developed and of the relative references is reported in Table 1. In this table the origin of the research group, the kind of relative motion between the magnet and the regenerator, the maximum magnetic field, the regenerator's volume, the frequency of the magnetization/demagnetization process, the magnetic material, the cooling

**Table 1**  
Summary of the experimental AMR systems.

Research group	Conf.	$\mu_0 H$ (T)	No. beds	Reg. vol. (cm <sup>3</sup> )	Freq. (Hz)	Regen. material	Qc (W)	$\Delta T$ (K)	Regen. geom.	Ref.
US Navy Univ. Vittoria	Alter.	7 (E)	1	173	0.01	Gd	0	40	Ribbon (0.2 mm)	[37]
	Alter./rotat.	2(S)	2	74	1	Gd,	0	50	Crushed part. (0.25–0.65 mm)	[38–41]
		2(S)		74	1	GdTb,	0	50	Spheres (0.2 mm) crushed part.	
		2(S)		74	1	GdEr	0	50		
		2(S)		49	0.8	Gd	0	15.5		
		2(S)		25	0.6	Gd	7	14		
Chubu electric/Toshiba	Alter.	2(S)		25.8	0.85	Gd–GdEr	35	12		
		5(S)		25.8	0.85	Gd–GdEr	35	6		
		4(S)	2	484	0.167	Gd	100	26	Spheres (0.3 mm)	[42]
		2(S)					40	24		
		5(S)					100	38	Spheres (0.15–0.3 mm)	[43]
Astronautics USA	Alter.		2	600	0.167	Gd	600	0		
Astronautics USA	Rotat.	1.5 (P)	6	33	4	Gd	15	14	Spheres (0.43–0.5 mm)	[44]
						GdEr	27	14	Spheres (0.25–0.4 mm)	
Astronautics USA	Rotat.	1.5 (P)	12	242	2	Gd	220	0	Plates	[45]
							155	8		
Astronautics USA	Rotat.	1.5 (P)	12	113	2	Gd	844	0	Spheres	[46]
							400	8.1		
Grenoble Nanjing University	Alter.	0.8 (P)	1	32	0.42	Gd	9	4	Plates	[47]
	Alter.	1.4 (P)	2	200	0.25	Gd	0	23	Spheres (0.2 mm)	[48]
						Gd <sub>5</sub> Si <sub>2</sub> Ge <sub>2</sub>	0	10		
Tokyo Institut of Techology/ Chubu	Rotat.	1.1 (P)	4	844	0.39	GdSiGeGa	0–40	25–5		
						GdDy	540	0.2	Spheres (0.5 mm)	[49]
							150	5.2		
Xi'an Jiaotong University	Alter.	2.2(S)	1	200	0.1	Gd	19	4	Spheres (0.15–0.3 mm)	[50,51]
						Gd <sub>5</sub> Si <sub>2</sub> Ge <sub>2</sub>	10	3	Part. (0.3–0.75 mm)	
Technical University of Denmark	Rotat.	1.24 (P)	24	570	2	Gd	0	25.4	Spheres (0.25–0.8 mm)	[52,53]
University of Western Switzerland	Alter.	1.45 T (P)	2	101	0.5	Gd	100	21	Plates	[54]
							0	22		

NB  $\mu_0 H$ : S, superconducting magnet; E, elettromagnet; P, permanent.

power, the temperature span of the system, the regenerator geometry, the reference are specified.

The University of Victoria prototype consists of two regenerators beds that are moved linearly through a magnetic field that is generated by a stationary superconducting solenoid magnet (maximum field of 5 T). The heat transfer fluid is helium and the regenerator is made of Gd and its alloys (multi-layer bed). Using a Gd bed, the prototype produced 7 W of cooling power. A no-load temperature span of 51 K is achieved with a multi-layer bed.

In 2007 Tura and Rowe develop a novel AMR using two nested Halbach arrays. They made a step forward compactness, higher operating frequencies, higher power densities, lower cost, and a much simplified design. The prototype, using 110 g of Gadolinium as a refrigerant, performed with a maximum temperature span under no thermal load of 29 °C, and 10 °C under 50 W. Overall COP is low, when compared with conventional refrigeration units, ranging between 0.3 and 0.8 for the most part while the maximum value is 1.6.

In 2011 Arnold, Tura and Rowe develop experiments with an active magnetic regenerator composed of two layer of Gd and Gd<sub>0.85</sub>Er<sub>0.15</sub> with a magnetic field of 2 and 5 T. the calculated COP values is 2.4 with a temperature span of 6 K using 5 T and 0.7 with a temperature span of 12 K at 2 T.

The Chubu/Toshiba AMR has two regenerator beds that are moved linearly in the presence of a magnetic field that is generated by a superconducting solenoid (with a magnetic field variable between 2 and 4 T). The heat transfer fluid is a mixture of water and ethanol. The cooling power is 100 W with a COP of 5.6 when the

system operates between 276 and 302 K. However, the reported COP is somewhat misleading because it does not include the work pump that move the secondary fluid and also neglects the power that is required to cool the superconducting solenoid.

Astronautics Corporation of America's first near room temperature AMR prototype was a reciprocating device with a 5 T magnetic field generated by a superconducting solenoid. Two regenerators were made of Gd. A cooling power of 100 W was achieved from his device with a temperature span of 38 K. Although the original device produced a relatively large cooling power over a large temperature span, the device itself was quite large and uses a superconducting magnet and therefore would not be practical as a commercial product.

In 2001, Astronautics built a second device that uses a more practical 1.5 T permanent magnet. The device uses a rotating regenerator divided into six separated beds. The regenerator is made of single magnetic material (Gd and LaFeSiH) and of different materials arranged in a multi-layer configuration (Gd–Er alloys). The cooling power, with a temperature span of 14 K, is 15 W with the Gd regenerator and 27 W with a multi-layer bed. The regenerator bed made of LaFeSiH material produces a lower cooling power. In 2007, a third generation rotary device that uses a rotating permanent magnet with 12 stationary bed made of Gd has been built. Experimental tests report cooling powers of 155 and 220 W with a temperature span of 8 K. In 2010 a device using stationary regenerator beds and rotating permanent magnet was shown to produce a maximum cooling power of 844 W at zero temperature span and 400 W at a temperature span of 8.1 K using 0.89 kg regenerator of

Gd. This device operates continuously with a maximum reported operating frequency of 4.7 Hz.

Nanjing University built a reciprocating device consisting of two regenerator beds moving linearly into and out of the magnetic field generated by a stationary 1.4 T permanent magnet. The beds are made of Gd and with first order magnetic materials (GdSiGeGa and GdSiGe). The experimental results report a no-load temperature span of 23 K with Gd, 25 K with GdSiGeGa and 10 K with GdSiGe.

The Tokyo Institute of Technology system is a rotary device that uses a rotating magnet with a stationary regenerator made of Gd–Dy alloys. The permanent magnet produces a magnetic field of 1.1 T. The system produces a cooling load of 150 W with a temperature span of 5.2 K.

The Xi'an Jiaotong University built a reciprocating AMRR with a single regenerator bed that uses a 2.18 T electromagnet. The regenerator's bed is made of Gd and GdSiGe alloys. The cooling power is 18.7 W with a Gd bed and 10.3 W with the first order magnetic material bed with a temperature span of 3 K.

In 2011 at the Department of Energy Conversion and Storage in Denmark an AMR high frequency rotary device has been assembled. The prototype is a ring of magnetocaloric material rotating in the gap of two concentric cylindrical permanent magnets. The peak flux density of magnets is around 1.24 T in a Halbach configuration. The regenerator is made of 24 regenerators bed with packed spheres of gadolinium. Deionized water mixed with 25% ethylene glycol is used as heat transfer fluid. The maximum temperature span measured at no-load, operating at 2 Hz, was 25.4 K. The machine was able to absorb 100 W cooling load at a temperature span of 21 K. A COP of 1.8 was measured for a cooling power of 400 W and a temperature span of 8.9 K.

In 2012 at the University of Applied Sciences of Western Switzerland a new type of reciprocating magnetic refrigerator has been built. This device use a NdFeB permanent magnet in Halbach configuration with a magnetic field of 1.45 T. The magnetic material used is Gadolinium in flat plates. The tested secondary fluids are: silicon oil, water and zitrec. The preliminary tests show that by using water or Zitrec as a secondary fluid a temperature span of 22 K with no load can be achieved with an operating frequency of 0.5 Hz.

Between the experimental devices developed, most of them have low cooling power and low energetic performances and therefore are not useful for practical applications. Therefore attention should be paid on the development of a new experimental prototype characterized by a greater cooling power (for commercial applications) and by energetic performances greater than those of a traditional vapour compression plant.

To this aim an optimal regenerator must be designed. This goal can be achieved utilizing an optimum magnetocaloric refrigerant. The development of a mathematical model able to simulate the thermal behaviour both of the secondary fluid and of the magnetic material, could allow to find an optimal configuration so that to be able to build subsequently an experimental prototype.

Different analytical model have been developed in order to evaluate the potential of an AMR refrigerator system. Most of them are mono-dimensional with gadolinium as magnetic material and water as a secondary fluid. In the follow reference will be made to the more recent models.

Engelbrecht et al. have presented a one-dimensional model using as magnetic material gadolinium and its alloys and as secondary fluid water [55,56].

Dikeos and Rowe [57] developed a numerical model using as magnetic material for the simulation Gd and DyAl<sub>2</sub>. This Research group introduced a mathematical model to investigate the demagnetizing effect in a single-material AMR [58,59].

A time and spatially dependent model was developed by Shir et al. [60]. The magnetic material was gadolinium and the secondary fluid a gas.

In the paper of Bouchekara et al. [61,62] an inverse approach is considered. Starting from the system performance required they developed an optimization process based on an AMR model. The magnetic material was gadolinium, the secondary fluid water.

Two and three dimensional models have been also presented [63–65]. Most of them are for flat plate regenerators. For these models the computation time may be prohibitive and the possibility of varying the regenerator geometry is limited. A comparison between the monodimensional and two dimensional models show excellent agreement for packed sphere regenerators and for flat parallel plates regenerators with thin regenerator channels [66].

### 3. The Active Magnetic Regenerator (AMR)

In the 1982 a new concept was introduced by Barclay [67] known as the Active Magnetic Regenerator (AMR). Unlike previous gas cycles, or magnetic cycles, the AMR concept coupled what had been two separate processes into a single one. Instead of using a separate material as a regenerator to recuperate the heat from the magnetic material, the AMR concept made use of the refrigerant itself as the regenerator. In essence, a temperature gradient is established throughout the AMR and a fluid is used to transfer heat from the cold end to the hot end. This subtle but essential idea produced a new magnetic cycle distinct from Carnot, Ericsson, Brayton, or Stirling. In the AMR, each section of the regenerator bed undergoes its own cycle; the entire mass of working material experiences a similar cycle but no longer at uniform temperature. An active magnetic regenerator can provide larger temperature spans with adequate heat transfer between the regenerator matrix and fluid. Examples of regenerator geometries are parallel plates, perforated plates or the most common packed bed of particles. The secondary fluid transport heat to and from the solid regenerator and can be water, water/anti-freezing mixtures, alcohol, helium, etc.

In this study the magnetic Brayton cycle has been considered, which is shown in Fig. 1. A complete cycle consists of two isentropic (adiabatic magnetization/demagnetization) steps and two isofield steps (cold and warm flows). The magnetic material cycles between the magnetic field of  $B_0$  and  $B_1$  and the temperature of high and low heat source,  $T_h$  and  $T_c$  respectively. During the isofield cooling process (1–2) the magnetic refrigerant expels heat while, during the isofield heating process (3–4) the magnetic refrigerant adsorbs heat. The magnetization and the demagnetization do not

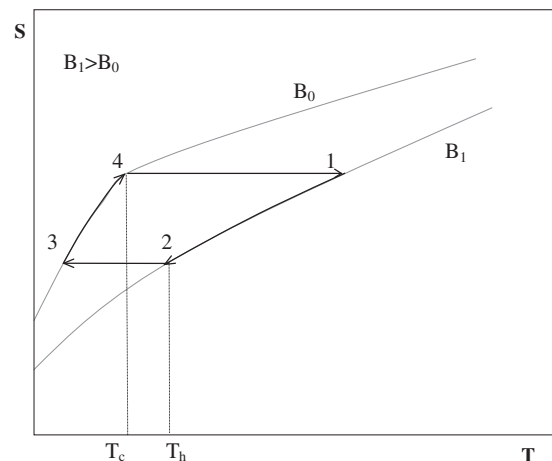


Fig. 1. Magnetic Brayton regenerative cycle.

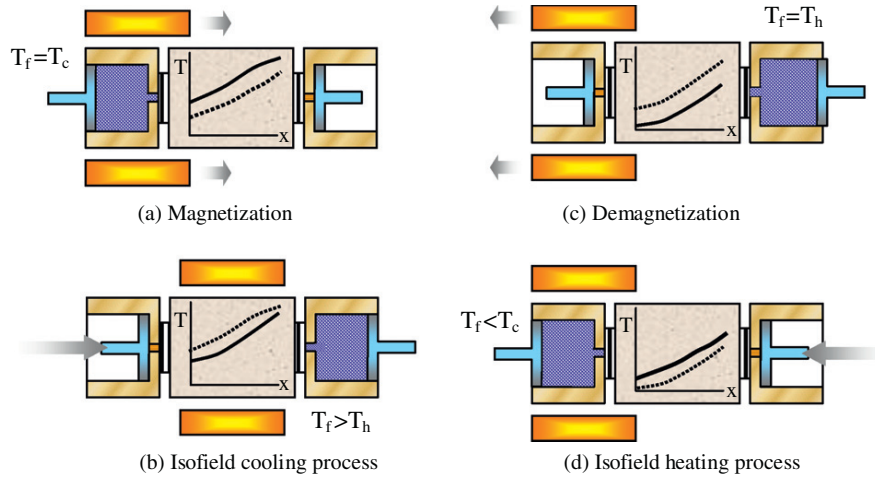


Fig. 2. Four schematic processes of an AMR cycle: solid and dashed lines referred to final and initial temperature profile respectively.

allow heat flow in and out of the magnetic refrigerant. The working principle of an AMR is presented in Fig. 2. For instance, let's assume that the bed is at a steady state condition with the hot heat exchanger at  $T_h$  and the cold heat exchanger at  $T_c$ . Four processes are present in the AMR cycle: (a) adiabatic magnetization: each particle in the bed warms up; (b) isofield cooling: the high field is present, the fluid is blown from the cold end to the hot end, and it absorbs heat from the bed and expels heat at a temperature higher than  $T_h$  in the hot heat exchanger; (c) adiabatic demagnetization: each particle in the bed cools again; (d) isofield heating: the field is zero, the fluid is blown from the hot end to the cold end, and it expels heat to the particles of the bed and absorbs heat at a temperature lower than  $T_c$  in the cold heat exchanger. In Fig. 2 the dashed line represents the initial temperature profile of the bed in each process while the solid line represents the final temperature profile of that process.

Essential for the design of an AMR cycle is the magnetic field generation. The magnetic field can be generated by a permanent magnet or an electromagnet. The upper limit of the magnetic field strength that can be achieved using a permanent magnet today is approximately 2 T. Magnetic field up to 2 T can be applied by an electromagnet. Within the electromagnets superconducting electromagnets can be also used. These consist in electromagnets cooled in order to reach very low temperature. In this temperature range the superconductivity can be utilized for magnetic field generation. However these configurations are not of practical interest because of the large currents that are required to generate useful magnetic fields for an electromagnet and because of the power required by cryogenic equipment necessary to maintain the superconducting temperature of a solenoid magnet (this power can greatly exceed the cooling power of small to medium scale AMR device). These configurations are therefore applicable only in the cryogenic temperature range or for test apparatus.

#### 4. The mathematical model

In order to analyze and design an optimum magnetic refrigeration system, it is important to model the magnetization and demagnetization process of the magnetic material and the regenerative warm and cold blow processes. The initial and the boundary conditions of each process connect each step of the four sequential processes to allow a cyclical operation of the AMR system [68–71].

##### 4.1. The model of magnetization and demagnetization processes

An entropy balance for the magnetocaloric solid refrigerant and the entrapped fluid in the porous matrix has been performed [72,73]:

$$dS = m_b \frac{C_B}{T_b} dT_b + v_b m_b \left( \frac{\partial M}{\partial T_b} \right)_H dB + m_f ds_f \quad (6)$$

To study the transient behaviour, ignoring the mass of the entrapped fluid compared to the mass of the magnetic material, the temperature variation is valuable integrating the following differential equation:

$$\left( \frac{\partial T_b}{\partial t} \right)_x = - \frac{T_b}{C_B} v_b \left( \frac{\partial M}{\partial T_b} \right)_H \frac{dB}{dt} \quad (7)$$

##### 4.2. The model of the magnetic material

According to Allab et al. [74], the upper limit of the magnetic field that can be achieved using a permanent magnet today is approximately 2 T; therefore, the properties of magnetocaloric materials are compared using a magnetic field change from 0 to 2 T.

###### 4.2.1. SOMT materials: Gd

The mean field theory describes the thermodynamic properties of a ferromagnetic material and can be used to calculate the magnetocaloric properties of gadolinium with acceptable accuracy. A simplified molecular theory allows the  $f(B, M, T) = 0$  state equation reported below for the magnetization [75,76]:

$$M(B, T) = Ng_J \mu_B B_J(X) \quad (8)$$

where

$$B_J(X) = \frac{2J+1}{J} \coth \left( \frac{2J+1}{2J} X \right) - \frac{1}{2J} \coth \left( \frac{X}{2J} \right) \quad (9)$$

is the Brillouin function based on the theory of the medium field of a magnetic material derived by a statistical approach and:

$$X = g \mu_B J \frac{B + \lambda M}{kT} \quad (10)$$

where  $\lambda$  is the Curie constant:

$$\lambda = \frac{3K}{Ng^2\mu_B^2J(J+1)}T_c \quad (11)$$

Implementing a simple iterative resolution, the magnetization versus the temperature at two values of the magnetic induction (0 and 2 T) has been obtained.

Since the numerical expression of the function  $M(B, T)$  is known, the total entropy of the gadolinium versus the temperature at two values of the external magnetic field has been derived.

At constant pressure, the entropy of a magnetic solid can be expressed as the sum of the magnetic, lattice and electronic contributions:

$$S(T, B) = S_m(T, B) + S_{lat}(T) + S_{el}(T) \quad (12)$$

The magnetic entropy is equal to:

$$s_m(B, T) = \frac{R}{M_m} \left[ \ln \frac{\sinh\left(\frac{2J+1}{2J}X\right)}{\sinh\left(\frac{X}{2J}\right)} - XB_J(X) \right] \quad (13)$$

The vibration electronic entropy is equal to:

$$s_{el}(T) = \frac{\gamma}{M_m} T \quad (14)$$

The last contribution to the entropy can be expressed as:

$$s_{lat}(T) = \frac{N_a R}{M_m} \left[ -3 \ln \left( 1 - e^{-\frac{T_{De}}{T}} \right) + 12 \left( \frac{T_{De}}{T} \right)^3 \int_0^{\frac{T_{De}}{T}} \frac{z^3}{e^z + 1} dz \right] \quad (15)$$

It is possible to obtain the specific heat versus the temperature at constant magnetic field, according the Maxwell equation:

$$c_B(B, T) = T \left( \frac{\partial s}{\partial T} \right)_B \quad (16)$$

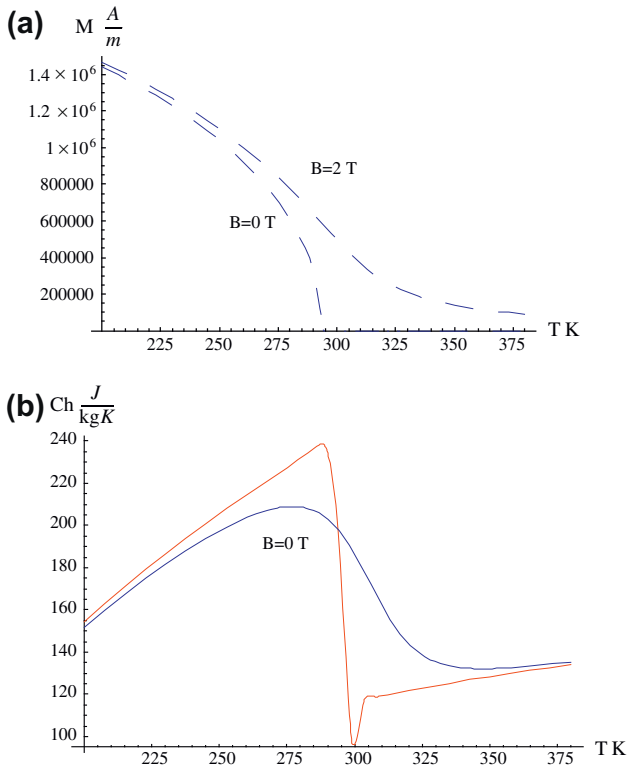


Fig. 3. The gadolinium specific heat (3 b) and magnetization (3 a) versus temperature at two values of the magnetic induction.

Table 2  
Magnetic and thermal parameters of Gd, Dy and Tb.

Element	g	J	$M_m$ (kg/mol)	$T_c$ (K)	$T_{De}$ (K)
Gd	2	3.5	0.157	294	173
Dy	1.33	7.5	0.163	179	180
Tb	1.5	6	0.159	230	177

In Fig. 3a and b the gadolinium magnetization and specific heat versus the temperature at two constant values of the magnetic field (0 and 2 T), are reported. In correspondence to the Curie temperature a strong reduction of the heat specific value is visible. The discontinuity of the specific heat is due to phase transition and the maximum corresponds at a temperature lower than the Curie temperature [77,78].

Comparing the numerical results for Gd [79] obtained with theoretical model and experimental results supplied by others [80,81], a good compromise has been found. The values of the specific heat calculated in this study are comprised the theoretical values indicated by Yu et al. [81], and the experimental ones reported by Peksoy and Rowe [80]. The oscillations are apparently due to both the different values used for the characteristics constants in the calculus of the specific heat and to the impurity of the materials used for experiments. The mean field model is advantageous because it generate thermodynamically consistent property data at any practical magnetic field and temperature. The maximal deviation between the experimental and theoretical data is in proximity of the Curie temperature. Therefore the molecular field model is an effective method with relatively high precision except for the critical region near  $T_c$ .

#### 4.2.2. SOMT materials: Gd based alloys

From the mean field theory the magnetic properties of  $Gd_xR_{1-x}$  (where R is another lanthanide metal) with the de Gennes model can be obtained.

The values for Gd, Dy and Tb parameters  $g, J, M_m, T_c, T_{De}$  used in the calculations are presented in Table 2.

From these data, the parameters of the different  $Gd_xDy_{1-x}$  and of the different  $Gd_xTb_{1-x}$  alloys, varying the composition, can be evaluated by interpolation and considering the following relationships:

$$\bar{G} = xG_{Gd} + (1-x)G_{Tb} \quad (17)$$

$$\bar{G} = xG_{Gd} + (1-x)G_{Dy} \quad (18)$$

$$\bar{\mu}^2 = x\mu_{Gd}^2 + (1-x)\mu_{Tb}^2 \quad (19)$$

$$\bar{\mu}^2 = x\mu_{Gd}^2 + (1-x)\mu_{Dy}^2 \quad (20)$$

where  $G$  is the de Gennes factor and is defined as:

$$G = (g-1)^2J(J+1) \quad (21)$$

and  $\mu$  is the effective magnetic moment defined as:

$$\mu = g\sqrt{J(J+1)} \quad (22)$$

Therefore from Eqs. (21) and (22) one can deduce the corresponding  $g$  and  $J$  for a given alloy. The Curie temperature of the alloy is evaluated as:

$$\bar{T}_c = 46\bar{G}^{2/3} \quad (23)$$

In Fig. 4 the  $Gd_{0.95}Dy_{0.05}$  specific heat versus the temperature at two constant values of the magnetic field (0 and 2 T), is reported. The Curie temperature of these alloys has been found 284 K. In

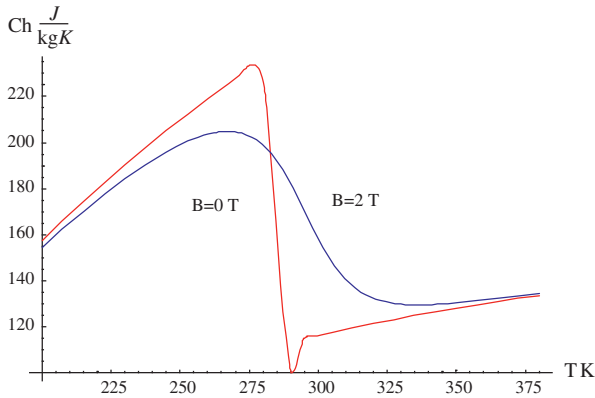


Fig. 4. The  $Gd_{0.95}Dy_{0.05}$  specific heat versus the temperature at two values of the magnetic field.

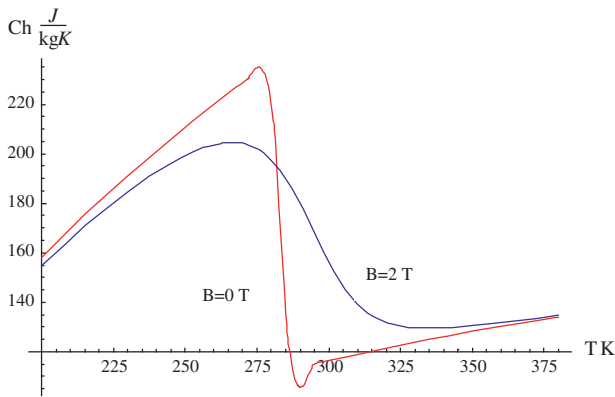


Fig. 5. The  $Gd_{0.9}Tb_{0.1}$  specific heat versus the temperature at two values of the magnetic field.

correspondence to the Curie temperature a strong reduction of the heat specific value is visible [82].

In Fig. 5 the  $Gd_{0.9}Tb_{0.1}$  specific heat versus the temperature at two constant values of the magnetic field (0 and 2 T), is reported. The Curie temperature of these alloys has been found 283 K.

Smaili and Chahine [83] show in their paper this model for Gd–Dy alloys. A comparison between the numerical data obtained with the de Gennes model and the experimental ones of the Curie temperature and of the isothermal magnetic entropy variation of the alloy  $Gd_xTb_{1-x}$  has been performed [84–86]. The comparison shows satisfactory agreement.

#### 4.2.3. FOMT materials: $Gd_5Si_2Ge_2$

The giant magnetocaloric effect in  $Gd_5Si_2Ge_2$  is associated with a reversible FOMT, during which the ferromagnetic to paramagnetic transition is coupled with the crystallographic phase change from the orthorhombic  $Gd_5Si_4$ -type to the monoclinic  $Gd_5Si_2Ge_2$ -type crystal structure [87].

A lot of experimental data are available in open literature for the  $Gd_5Si_2Ge_2$  alloy [88–92]. To evaluate the MCE of this alloy a good method is to fit curves of the specific heat at each magnetic field. For the AMR model the magnetocaloric material properties should be smooth and thermodynamically consistent. Therefore, experimental data generally has to be smoothed before it can be used by the model; the curve fitting of experimental data accomplishes this smoothing by curve fitting which has the additional

benefit of providing a computationally efficient, analytical model of entropy.

The first step in obtaining a curve of specific heat as a function of temperature is to separate the lattice portion of the data from the magnetic portion of the data. The magnetic specific heat data can be fitted with a Gaussian curve for each magnetic field value.

The experimental data for specific heat available from literature are reported in Fig. 6, data are available for a magnetic field of 0 and 2 T.

The equation of the curve for the specific heat with zero magnetic field can be expressed as:

$$C_B(0, T) = -48.966 + 34.512 \log_{10}(T) + \frac{139}{\sqrt{2\pi}} e^{-\frac{1}{9}(T-276)^2} + \frac{5}{\sqrt{2\pi}} e^{-0.71(T-299)^2} - \left( \frac{1}{1 + e^{-10^4(T-280)}} \right) 1.28 \log_2((T-279)^2) - \left( \frac{1}{1 + e^{-10^4(T-300)}} \right) 10^{-2} T \quad (24)$$

The equation of the curve for the specific heat with 2 T magnetic field can be expressed as:

$$C_B(2, T) = -48.966 + 34.512 \log_{10}(T) + \frac{114}{\sqrt{2\pi}} e^{-\frac{1}{9}(T-283)^2} - \left( \frac{1}{1 + e^{-10^4(T-280)}} \right) 0.55 \log_2((T-279)^4) \quad (25)$$

These expressions can be used in order to calculate the entropy of the magnetic material in accordance with Eq. (16).

The magnetization of this compound has been evaluated by means of a set of experimental isothermal magnetization curves measured increasing and decreasing the magnetic field [88–90]. Therefore the model takes into account the hysteresis effect. As a consequence of hysteresis the adiabatic transformations are not parallel to the one computed with reversible processes and the irreversibility makes the cycle asymmetrical.

In this paper the evaluation of  $\Delta T_{ad}$  is indirect, based on heat capacity measurements. As noted by Gschneidner et al. [93] a FOMT material presents some problems when determining the  $\Delta T_{ad}$  by either direct or indirect methods. Indeed, the kinetics of the first-order transformation may be slow and a rapid magnetic field change may not be slow enough to allow the transformation to go to completion.  $\Delta T_{ad}$  values obtained from indirect measurements are based on experiments in equilibrium or quasi-equilibrium conditions. But in most magnetic refrigerators magnetization and demagnetization steps may become non-equilibrium processes.

#### 4.2.4. FOMT materials: $MnAs_{1-x}Sb_x$

A theoretical investigation based on the Bean and Rodbell model [84,85,94,95] can be used to describe the giant magnetocaloric effect of  $MnAs_{1-x}Sb_x$  compounds in the vicinity of the first order phase transition. The model considers the dependence of the critical magnetic phase transition temperature on the volume change expressed as follow:

$$T_c = T_o(1 + \beta\omega) \quad (26)$$

where  $\omega$  is the cell deformation,  $\beta$  measures the slope of the Curie temperature curve on the cell deformation and  $T_o$  is the Curie temperature in absence of deformation. The state equation for magnetization is:

$$M(B, T) = Ng_j \mu_B J_B J_j(X) \quad (27)$$

where  $J_B$  is the Brillouin function. In this case  $X$  can be defined as:

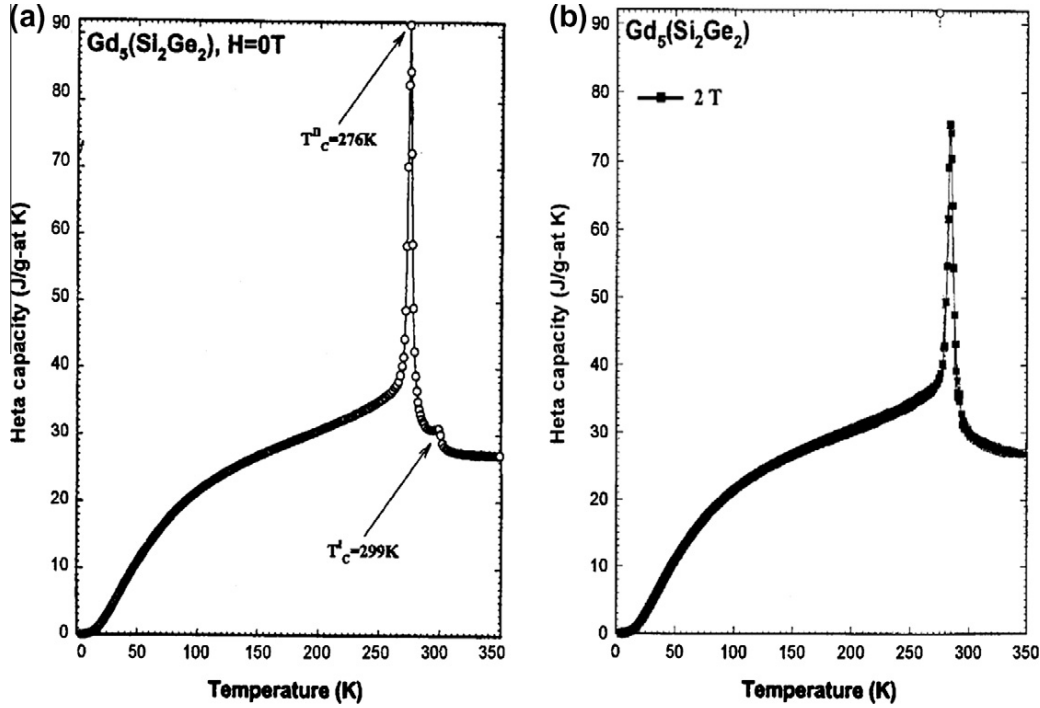


Fig. 6. Specific heat of Gd<sub>5</sub>(Si<sub>2</sub>Ge<sub>2</sub>) as a function of temperature for a magnetic field of 0 T (6a) and 2 T (6b).

$$X = \frac{1}{T} \left[ 3T_0 \left( \frac{J}{J+1} \right) B_J + \frac{g_J \mu_B J}{k} B + \frac{9}{5} \left( \frac{(2J+1)^4 - 1}{(2J+2)^4} \right) T_0 \eta B_J^3 \right] \quad (28)$$

The last term in the argument of the Brillouin function comes from the elastic deformation. The parameter  $\eta$  controls the order of the magnetic phase transition and is given by:

$$\eta = \frac{5}{2} \frac{[4J(J+1)]^2}{[(2J+1)^4 - 1]} NkKT_0 \beta^2 \quad (29)$$

where  $K$  is the compressibility factor. From the Landau theory of phase transition, the condition  $\eta > 1$  leads to a first order magnetic phase transition, while  $\eta < 1$  leads to a second order phase transition. If  $\eta = 0$  the Brillouin function presents only the linear term and the phase transition is of second order and occurs at the Curie temperature  $T = T_0 = T_c$ .

A comparison between the adiabatic temperature variation in the vicinity of the transition temperature under a change of external magnetic field from 0 to 2 and 5 T obtained with the theoretical model and with experimental values has been performed [85,96]. The theoretical values are in good agreement with experimental data.

**Table 3**  
Model parameters for MnAs<sub>1-x</sub>Sb<sub>x</sub> compounds with different Sb concentrations.

$x$	$T_c$	$T_0$	$\eta$
0	317	293	2
0.05	300	287	1.65
0.1	282	277	1.4
0.125	271	266	1.37
0.15	259	255	1.35
0.2	246	243	1.3
0.25	235	232	1.25
0.3	223	220	1.35
0.4	214	214	0.8

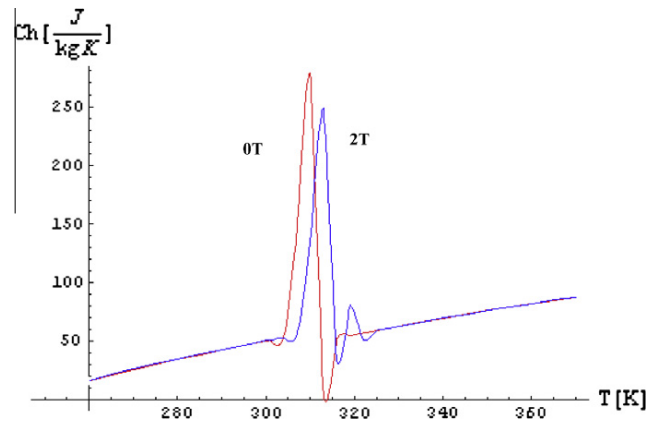


Fig. 7. MnAs<sub>0.9</sub>Sb<sub>0.1</sub> specific heat versus the temperature for a magnetic field of 0 and 2 T.

In Table 3 are reported the two model parameters  $T_0$  and  $\eta$  used to fit the experimental data from a comparison with the theoretical results for different Sb concentrations. For concentrations  $x = 0, 0.1, 0.15, 0.25, 0.30$  the model gives  $\eta > 1$ , which is the condition for the existence of a first order magnetic phase transition. As higher the  $\eta$  values as stronger will be the first order magnetic phase transition [96].

In Fig. 7 the MnAs<sub>0.9</sub>Sb<sub>0.1</sub> specific heat versus the temperature at two constant values of the magnetic field (0 and 2 T), is reported.

In Fig. 8 the MnAs<sub>0.95</sub>Sb<sub>0.05</sub> specific heat versus the temperature at two constant values of the magnetic field (0 and 2 T), is reported.

#### 4.3. The model of the regenerative warm and cold blow processes

The analysis and equations in this section are based on the following simplifying assumptions:

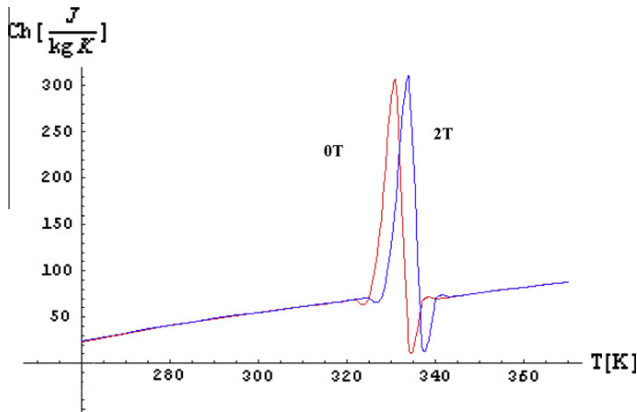


Fig. 8. MnAs<sub>0.95</sub>Sb<sub>0.05</sub> specific heat versus the temperature for a magnetic field of 0 and 2 T.

1. The temperature of the secondary fluid entering at each end of the refrigerant bed is constant. The secondary fluid exchanges thermal energy with the environment thanks to two heat exchangers not considered in the present mathematical model. The heat exchangers are expected to be very efficient (with an infinite heat exchange area), such that the secondary fluid alternatively flowing from the heat exchangers into the refrigerant bed is cooled until a temperature of  $T_h$  and is heated until a temperature of  $T_c$ .
2. The bed is assumed adiabatic towards the environment.
3. The magnetic material is isotropic.
4. The fluid flow through the bed is parallel and uniform throughout any cross section. The temperature change perpendicular to the main flow direction can be therefore neglected and the problem can be considered one-dimensional.
5. The fluid pressure drop throughout the bed has been neglected.
6. The regenerator surface area is evenly distributed throughout its volume.
7. The solid spheres are of uniform shape and incompressible.

Based on the above assumptions, an energy balance for the secondary fluid and for the magnetic material can be performed, which results in two partial differential equations [97–101]:

$$\begin{cases} m_f C_f \frac{\partial T_f}{\partial t} + \dot{m}_f L C_f \frac{\partial T_f}{\partial x} - ALK_{eff,f} \frac{\partial^2 T_f}{\partial x^2} = hA_{sc}(T_b - T_f) \\ m_b C_b \frac{\partial T_b}{\partial t} - ALK_{eff,b} \frac{\partial^2 T_b}{\partial x^2} = hA_{sc}(T_f - T_b) \end{cases} \quad (30)$$

The surface area of the packed bed which appears in both energy equations is developed based on geometrical considerations and is defined as [102–104]:

$$A_{sc} = \frac{6}{d_p} V(1 - \varepsilon) \quad (31)$$

The formulation of the fluid-to-solid heat transfer coefficient in this study is based on the Wakao et al. [105,106] empirical correlation:

$$h = \frac{k_f}{d_p} \left[ 2 + 1.1 Pr_f^{1/3} \left( \frac{\rho_f w_f d_p}{\mu_f} \right)^{0.67} \right] \quad (32)$$

In the present study, the dispersion phenomenon is treated as an additional diffusive term added to the stagnant component [107]. The stagnant component is expressed in terms of phase porosities and the individual thermal conductivities of the phases. The empirical correlation developed by Wakao and Kagueli [106] is employed in this study to model the effective conductivities [108].

$$K_{eff,f} = \varepsilon k_f + 0.5 \left[ Pr_f \left( \frac{\rho_f w_f d_p}{\mu_f} \right) \right] k_f \quad (33)$$

$$K_{eff,b} = (1 - \varepsilon) k_s$$

#### 4.4. The boundary and the initial conditions of the AMR cycle

The boundary and initial conditions for the Eqs. (7) and (30), will be presented below for each phase of the cycle. In demagnetization, at  $t = 0$ , the bed is subjected to a magnetic field  $B_{max}$ . The magnetic field is nullified, according to the function  $B(t)$ , at  $t = t_D$ . Using the Eq. (7) with the initial condition:

$$T_b(0, x) = T_{b,HF}(x) \quad (34)$$

a new temperature profile is obtained:

$$T_{b,D}(x) = T_b(t_D, x) \quad (35)$$

In the last step ( $t_D < t \leq t_{CF}$ ) in the absence of the magnetic field, the fluid is blown from the hot end to the cold end of the bed. The secondary fluid enters the hot side of the bed at temperature equal to  $T_h$ . The secondary fluid contained in the bed at the time  $t = t_D$  presents the same temperature profile reached at the time  $t = t_D + t_{CF} + t_M + t_{HF}$ . Considering the Eq. (30) with the following initial and boundary conditions:

$$\dot{m}(t) = -\dot{m}_0 \quad (36)$$

$$T_f(t_D, x) = T_{f,HF}(x) \quad (37)$$

$$T_b(t_D, x) = T_{b,D}(x) \quad (38)$$

$$T_f(t, L) = T_h \quad (39)$$

$$\frac{\partial T_f}{\partial x}(t, 0) = 0 \quad (40)$$

$$\frac{\partial T_b}{\partial x}(t, 0) = 0 \quad (41)$$

$$\frac{\partial T_b}{\partial x}(t, L) = 0 \quad (42)$$

The new temperature profiles for the bed and for the regenerating fluid are determined:

$$T_{b,CF}(x) = T_b(t_D + t_{CF}, x) \quad (43)$$

$$T_{f,CF}(x) = T_f(t_D + t_{CF}, x) \quad (44)$$

In the magnetization phase ( $t_{CF} \leq t \leq t_M$ ), the bed is magnetized increasing the magnetic field, until  $B_{max}$ , according to a linear evolution.

Using the Eq. (7) with the following initial condition:

$$T_b(t_D + t_{CF}, x) = T_{b,CF}(x) \quad (45)$$

a new temperature profile of the bed is obtained:

$$T_{b,M}(x) = T_b(t_D + t_{CF} + t_M, x) \quad (46)$$

In the fourth phase ( $t_M \leq t \leq t_{HF}$ ) the fluid is blown from the cold end to the hot end of the bed. The magnetic field is equal to  $B_{max}$  and the secondary fluid in the bed exhibits the same profile temperature showed at the time  $t = t_D + t_{CF}$ . The regenerating fluid passes through the bed entering at its cold side at temperature equal to  $T_c$ . Considering the Eq. (30) and the following initial and boundary conditions:

$$\dot{m}(t) = \dot{m}_0 \quad (47)$$

$$T_f(t_D + t_{CF} + t_M, x) = T_{f,CF}(x) \quad (48)$$

$$T_b(t_D + t_{CF} + t_M, x) = T_{b,M}(x) \quad (49)$$

$$T_f(t, 0) = T_c \quad (50)$$

$$\frac{\partial T_f}{\partial x}(t, L) = 0 \quad (51)$$

$$\frac{\partial T_b}{\partial x}(t, 0) = 0 \quad (52)$$

$$\frac{\partial T_b}{\partial x}(t, L) = 0 \quad (53)$$

The new temperature profiles for the bed and for the regenerating fluid are determined:

$$T_{b,HF}(x) = T_b(t_D + t_{CF} + t_M + t_{HF}, x) \quad (54)$$

$$T_{f,CF}(x) = T_f(t_D + t_{CF} + t_M + t_{HF}, x) \quad (55)$$

#### 4.5. Numerical solution

There is not analytical solution to solve for the equations presented previously. The Runge–Kutta explicit method has been used to solve the equations system. In this simulation a fourth stage stepping scheme has been adopted for the numerical solution, with a discretization of 50 steps in time and space integration. Because the model concerns a thermodynamic cycle two conditions have to be respected:

$$T_B(0, x) = T_B(t_D + t_{CF} + t_M + t_{HF}, x) \quad (56)$$

$$0 < COP < COP_{MC} \quad (57)$$

The Eq. (56) represents the regime conditions of the AMR, while the Eq. (57) represents the thermodynamic consistency. An iterative resolution of the Eqs. (7) and (30) provides the regime solution utilizing a tentative profile temperature of the magnetic bed

$$T_B(0, x) = T_{tr}(x) \quad (58)$$

The calculative cycle stops when the error  $\delta$  reported below is smaller than  $1 \times 10^{-6}$  K:

$$\delta = \text{Max}\{|T_B(0, x) - T_B(t_D + t_{CF} + t_M + t_{HF}, x)|\} \quad (59)$$

When the iterations stop the refrigeration energy and the energy supplied to the environment are calculated according to the following equations:

$$Q_{ref} = \int_{t_D}^{t_D+t_{CF}} \dot{m}(t) \bar{c}_f (T_c - T_f(t, 0)) dt \quad (60)$$

$$Q_{rej} = \int_{t_D+t_{CF}+t_M}^{t_D+t_{CF}+t_M+t_{HF}} \dot{m}(t) \bar{c}_f (T_f(t, L) - T_H) dt \quad (61)$$

To evaluate the mean powers it is necessary to consider the total cycle time:

$$\bar{Q}_{ref} = Q_{ref} \frac{1}{t_{tot}} \quad (62)$$

$$\bar{Q}_{rej} = Q_{rej} \frac{1}{t_{tot}} \quad (63)$$

The Ergun equation [109] reported below allows the evaluation of the pressure drop in secondary fluid flow:

$$\frac{\partial p}{\partial x} = 180 \left( \frac{1 - \varepsilon}{\varepsilon} \right)^2 \frac{\mu_f}{d_p} w_{inf} + 1.8 \left( \frac{1 - \varepsilon}{\varepsilon^2} \right) \frac{\rho_f}{d_p} w_{inf}^2 \quad (64)$$

Integrating Eq. (64) along the magnetic bed with regard to the time, the pressure drop is evaluated. The work of the pump can be expressed as:

$$W_p = \frac{\dot{m}(t)(\Delta p_{CF} + \Delta p_{HF})}{\eta_p \rho_f} (t_{CF} + t_{HF}) \quad (65)$$

Using these equations the Coefficient of Performance is valuable:

$$COP = \frac{Q_{ref}}{Q_{rej} - Q_{ref} + W_p} \quad (66)$$

## 5. Results and discussion

By means of the simulation with the previous equations, integrated with the boundary and the initial conditions, the refrigeration power, the Coefficient of Performance, the temperature profile of the magnetic bed and of the regenerating fluid have been obtained. In the simulation the temperature range that has been explored is 280–295 K. The secondary fluid used in this temperature range is liquid water. Indeed, in this temperature range water is the best secondary fluid because has low viscosity (therefore needs a low work of the pump) and high values of specific heat and of thermal conductivity.

The aim of this work is to make a comparison between first and second order magnetic material working in the same operating conditions. Therefore, the numerical program simulates a regenerator made of: pure Gd, Gd<sub>0.95</sub>Dy<sub>0.05</sub>, Gd<sub>0.9</sub>Tb<sub>0.1</sub>, Gd<sub>5</sub>Si<sub>2</sub>Ge<sub>2</sub>, MnAs<sub>0.9</sub>Sb<sub>0.1</sub>, MnAs<sub>0.95</sub>Sb<sub>0.05</sub>.

The cooling capacity of an AMR system can be varied by changing: the secondary fluid mass flow rate, the cycle time or both parameters simultaneously. The variation of the secondary fluid mass flow rate corresponds to a variation of the pump speed; the variation of the cycle time corresponds to a variation of fluid flow time that corresponds to a variation of the frequency of the pump motor speed.

In this paper to investigate the dependence of efficiency on cycle time and mass flow rate, the performance of an AMR cycle working with different magnetic materials is predicted over a range of secondary fluid mass flow rate and cycle times.

The parameters reported in Table 4 are used to carry out the simulation to investigate the effect on cycle performance of secondary fluid mass flow rate. In the simulation the fluid flow blow time was held constant.

Fig. 9a and b reports the refrigerating power and COP values as a function of the water mass flow rate for the different magnetic materials. In the graph 9a is reported the maximum COP referred to the Carnot cycle and the COP of a vapour compression plant working with the same operating conditions. The COP of the traditional vapour compression plant has been predicted with the DOE/ORNL Heat Pump model [110]. The Fig. 9a shows that for all

**Table 4**

Model parameters to investigate the effect of secondary fluid mass flow rate with the different magnetic materials.

Characteristics	Values	Dimensions
$d_p$	600	$\mu\text{m}$
$L$	0.2	m
$D$	0.045	m
$\varepsilon$	0.26	–
$B_{min}$	0	T
$B_{max}$	2	T
$t_D = t_M$	0.2	s
$t_{CF} = t_{HF}$	2	s
$T_H$	295	K
$T_c$	280	K

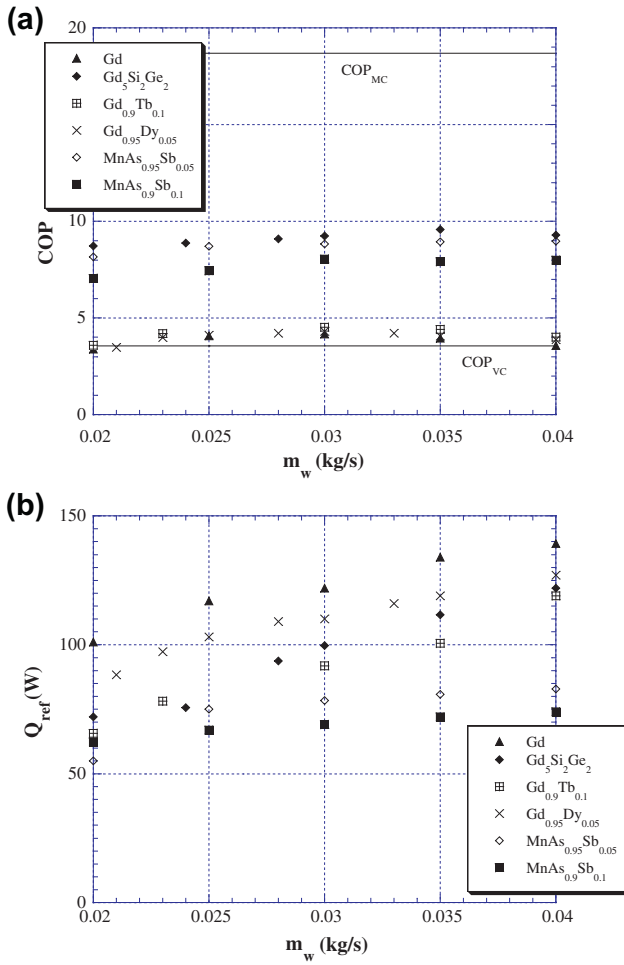


Fig. 9. COP (9 a) and refrigerating power (9 b) as a function of water mass flow rate for different magnetic materials.

magnetic materials the COP first increases with the water mass flow rate and after slightly decrease. Indeed, a greater water flow modifies the profile temperature of the bed, decreasing the temperature difference between the water and the magnetic material. Accordingly, the efficiency of the regenerator improves causing an increase of the refrigeration power and therefore increasing the COP. The work of the pump always increases with the fluid mass flow rate. When this effect prevails on the rise of the refrigeration power the COP decreases.

Therefore for each magnetic material there is a secondary fluid mass flow rate that maximizes the COP of the cycle.

The Fig. 9a clearly shows that with a regenerator made of first order magnetic phase transition material the COP is always better (from a minimum of 50 to a maximum of 60%). Indeed, from the theoretical results a FOMT material shows a greater magnetocaloric effect in terms of a greater adiabatic temperature variation, and therefore a greater COP.  $Gd_5Si_2Ge_2$  is the best FOMT material. Between the  $MnAs_{1-x}Sb_x$  compounds  $MnAs_{0.95}Sb_{0.05}$  shows a better COP than  $MnAs_{0.9}Sb_{0.1}$ . The latter compound has a lower  $\eta$  value. As higher is the  $\eta$  values as stronger will be the first order magnetic phase transition and therefore the magnetocaloric effect of the material. With FOMT material the COP is always greater than a vapour compression plant working in the same operating conditions (from a minimum of a 59 to a maximum of 62%).

In this paper the COP of FOMT materials is evaluated in a ideal case in which is assumed that the first-order transformation to go

to completion in the magnetization or demagnetization time. In a real machine based on an AMR cycle working with low operating frequencies the time to complete the first order transition may be great compared to the cycle time. In this case after the first cycle the magnetic refrigerant may consists of two phases and the entropy change may be lowered by a significant amount (the entropy change due to structural transformation accounts for about half of the total entropy change during magnetic ordering) [111]. Therefore the MCE may be decreased lowering the COP by a significant amount.

The SOMT materials show similar energetic performances slightly better than those of a vapour compression plant. Therefore the COP of the AMR cycle working with these materials needs an improvement.

Graph 9b shows the refrigerating power. An increase of the water mass flow rate increases the regenerator efficiency and therefore the refrigerating power. The simulation results clearly indicate that the refrigerating power of the SOMT materials is greater than that of the FOMT materials. In particular, Gd shows the greater refrigerating power, whereas  $MnAs_{0.9}Sb_{0.1}$  the lower one. Pure Gd and its alloys exhibit a significant magnetocaloric effect over a large temperature span, whereas for FOMT materials this effect is over a very small temperature range containing the Curie temperature.

The parameters reported in Table 5 are used to carry out the simulation to investigate the effect on cycle performance of cycle time. In the simulation the water mass flow rate was held constant.

Fig. 10a and b shows the COP and the refrigerant power values varying the fluid flow circulation time. Decreasing the latter parameter the mass of fluid flowing in the bed decreases at constant fluid mass flow rate. Corresponding to a small fluid mass, although the fluid can be regenerated to reach lower exit temperature, a small amount of transfer fluid can produce only a little refrigerating capacity. On the other hand, excessive transfer fluid perturbs the temperature profile of the AMR, decreasing the temperature difference between the fluid and the bed. The bed quickly becomes overwhelmed by the fluid flow and the efficiency of the heat transfer decreases quickly causing a loss in cooling power. Accordingly, it exists for each magnetic material a fluid circulation time value which provides maximum COP.

The energetic performances of FOMT materials are always better than those of SOMT ones (from a minimum of +40% to a maximum of +60%).

Corresponding to the lowest (less than 1 s) and highest (greater than 2 s) fluid blown period the SOMT materials outperform a traditional vapour compression plant. FOMT materials always have energy performance better than a traditional plant (from a minimum of +40% to a maximum of +62%).

In graph 10b the refrigeration power is reported. The refrigerating power always decreases increasing the flow period which increases the cycle time. Refrigeration power of SOMT materials is

Table 5

Model parameters to investigate the effect of cycle time with the different magnetic materials.

Characteristics	Values	Dimensions
$d_p$	600	$\mu\text{m}$
$L$	0.2	m
$D$	0.045	m
$\varepsilon$	0.26	-
$\dot{m}_w$	0.04	kg/s
$B_{min}$	0	T
$B_{max}$	2	T
$t_D = t_M$	0.2	s
$T_h$	295	K
$T_c$	280	K

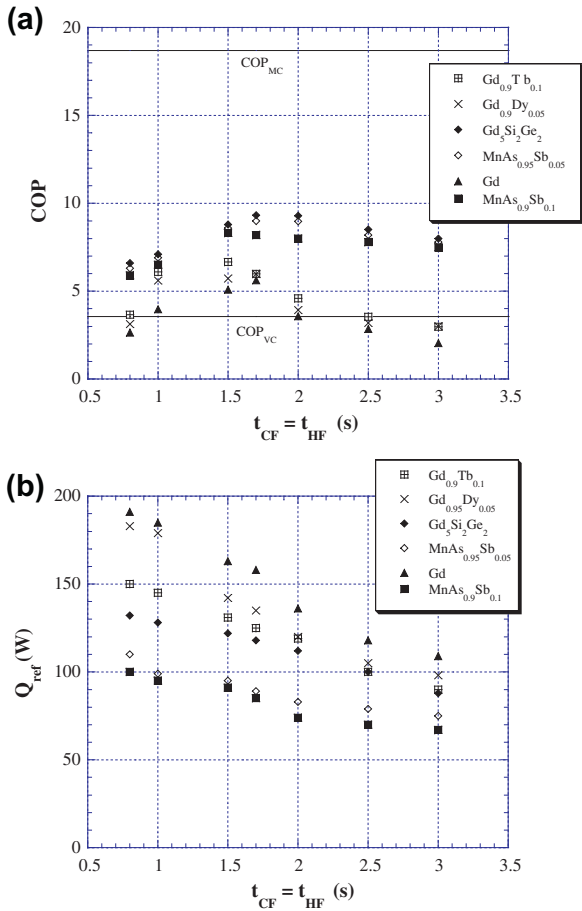


**Fig. 10.** COP (10 a) and refrigerating power (10 b) as a function of flow circulation time for different magnetic materials.

**Table 6**

Model parameters in the comparison between a Gd<sub>x</sub>Tb<sub>1-x</sub> layered bed with FOMT materials.

Characteristics	Values	Dimensions
$d_p$	600	$\mu\text{m}$
$L$	0.2	m
$D$	0.045	m
$\varepsilon$	0.26	–
$\dot{Q}_{ref}$	105	W
$B_{min}$	0	T
$B_{max}$	2	T
$t_D = t_M$	0.2	s
$T_h$	295	K
$T_c$	275	K

higher than that of FOMT materials all over the fluid flow time range.

To increase the COP an AMR cycle working with SOMT materials a layered regenerator bed can be utilized. The alloys of materials have a very convenient property to produce layered beds, namely that the Curie temperature changes with the fraction of change of the components. Therefore, a pure gadolinium regenerator exhibits a large magnetocaloric effect only over a small temperature range containing its Curie temperature. Using alloys it is possible to fabricate a layered bed composed of several magnetic alloys, each placed at the location in the regenerator where the average temperature is near its Curie temperature.

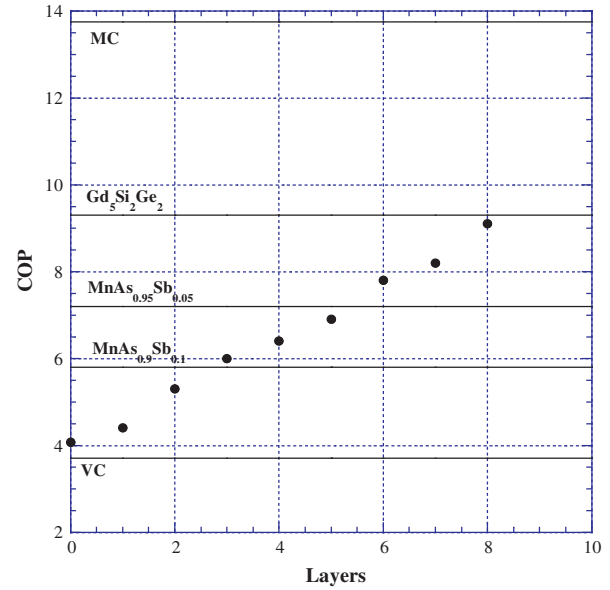


**Fig. 11.** COP as a function of layer's number of Gd<sub>x</sub>Tb<sub>1-x</sub> alloys in comparison with the different magnetic materials.

In the temperature range 275–295 K the Gd<sub>x</sub>Tb<sub>1-x</sub> alloys have been chosen as constituent materials for the regenerator. Water is used as a secondary fluid.

It is possible to make the bed of different numbers of layer each working at its optimal point selecting the composition of the alloy. An iterative procedure has been adopted in order to determine the optimal composition of each layer of the bed.

The parameters reported in Table 6 are used to carry out the simulation to make a comparison between a Gd<sub>x</sub>Tb<sub>1-x</sub> layered bed with FOMT materials. In the simulation the cooling capacity was held constant selecting the appropriate regenerating fluid mass flow rate.

Fig. 11 shows COP values varying the number of the bed's layer. In the graph the zero layer is referred to a bed made of pure Gd. In the graph is reported the maximum COP referred to the Carnot cycle (MC) and the COP of a vapour compression plant working with the same operating conditions (VC). The graph reports also COP values of FOMT materials (Gd<sub>5</sub>Si<sub>2</sub>Ge<sub>2</sub>, MnAs<sub>0.95</sub>Sb<sub>0.05</sub> and MnAs<sub>0.9</sub>Sb<sub>0.1</sub>).

The COP of the AMR cycle is an increasing function of the layer's number. Indeed, increasing the layers of Gd–Tb alloys, placing each layer at the location where the average temperature is near its Curie temperature, a larger magnetocaloric effect can be obtained. The non-layered bed shows worse energetic performances than the layered one and the COP is only slightly better than that of a vapour compression plant (+7.5%). Increasing the number of layers the COP increases of more than 56%.

Comparing the value of the COP of an 8 layers AMR cycle with that pertinent to a classical vapour compression plant, the AMR shows an energetic performance greater than about 60%.

Gd<sub>5</sub>Si<sub>2</sub>Ge<sub>2</sub> is the best magnetic material but its COP is only slightly better than that of a 8 layers regenerator (about 2%).

A multi-layer regenerator with more than 2 layers always over performs a MnAs<sub>0.9</sub>Sb<sub>0.1</sub> bed and multi-layer bed with more than 5 layers always over performs a MnAs<sub>0.95</sub>Sb<sub>0.05</sub> bed.

## 6. Conclusions

In the present paper, a practical model for predicting the performance and efficiency of an AMR refrigerator system has been

introduced. The model is able to simulate an AMR made of FOMT and SOMT materials. In particular: Gd,  $Gd_{0.95}Dy_{0.05}$ ,  $Gd_{0.9}Tb_{0.1}$  (SOMT) and:  $Gd_5Si_2Ge_2$ ,  $MnAs_{0.9}Sb_{0.1}$ ,  $MnAs_{0.95}Sb_{0.05}$  (FOMT) have been considered as solid magnetic refrigerants.

The model simulates both the magnetic material and the entire cycle of an AMR operating in conformity with a Brayton regenerative cycle in a temperature range of 280–295 K, in conformity with the room temperature range. The secondary fluid in this temperature range is liquid water. The model predicts the refrigeration capacity and the efficiency of the cycle.

To investigate the dependence of efficiency on cycle time and secondary fluid mass flow rate, the performance of an AMR refrigerator system, working with different magnetic materials, is predicted over a range of secondary fluid mass flow rate and cycle times.

For the range of operating conditions investigated, the simulation results lead to the following conclusions:

- (1) The results of the simulation can be used in an optimization of the design of an experimental prototype. The results clearly show that for each magnetic material there is a secondary fluid mass flow rate and cycle time that maximizes the COP of the cycle.
- (2) The energetic performances of the FOMT materials are always better than those of SOMT ones (from a minimum of +40% to a maximum of +60%).  $Gd_5Si_2Ge_2$  is the best magnetic material in this temperature range. FOMT materials always have energetic performance better than a traditional plant working in the same operating conditions (from a minimum of +40% to a maximum of +62%). In this paper the COP of FOMT materials is evaluated in an ideal case in which is assumed that the first-order transformation to go to completion in the magnetization or demagnetization time
- (3) The SOMT materials show energetic performances similar or slightly better than those of a vapour compression plant. Therefore with these materials a layered regenerator bed is a good solution to increase the COP of the whole plant.

In order to increase the COP an AMR cycle working with SOMT materials a layered regenerator bed can be utilized. A simulation has been carried out in order to compare the energetic performances of a SOMT layered bed with those of FOMT materials.

In the temperature range 275–295 K the  $Gd_xTb_{1-x}$  alloys have been chosen as constituent materials for the regenerator. Water is used as a secondary fluid. The simulation results lead to the following conclusions:

- (1)  $Gd_5Si_2Ge_2$  is the best magnetic material but its COP is only slightly better than that of a 8 layers regenerator (about 2%).
- (2) A multi-layer regenerator with more than 2 layers always over performs a  $MnAs_{0.9}Sb_{0.1}$  bed.
- (3) A multi-layer bed with more than 5 layers always over performs a  $MnAs_{0.95}Sb_{0.05}$  bed.
- (4) An 8 layers AMR cycle shows an energetic performance greater than that of a vapour compression plant of about 60%.

These results indicate that magnetic refrigeration is a promising refrigeration technology that will be used in chiller applications. The MCE of magnetic materials is so important in magnetic refrigeration that most work is directed to investigating and searching for new magnetic materials of large MCE. The model presented is a good instrument to investigate the energetic performances of FOMT and SOMT materials in different operating conditions in an AMR cycle. FOMT materials give better energetic performances but give problems in practical use. Problems are related to: a large

time required for the adiabatic temperature variation varying the magnetic field, a significant hysteresis, a large volume change in phase transition. In this paper the COP of FOMT materials is evaluated in an ideal case in which is assumed that the first-order transformation to go to completion in the magnetization or demagnetization time. Problems also arise with the preparation and the cost connected with a large scale production.

SOMT materials in multi-layer beds show energetic performances comparable with those of FOMT materials with less problems in practical use.

## References

- [1] Aprea C, Greco A. An experimental evaluation of the greenhouse effect in R22 substitution. *Energy Convers Manage* 1998;39(9):877–87.
- [2] Sekhar SJ, Kumar KS, Lal DM. Ozone friendly HFC134a/HC mixture compatible with mineral oil in refrigeration system improves energy efficiency of a walk in cooler. *Energy Convers Manage* 2004;45(7–8):1175–86.
- [3] Park KJ, Shin YB, Jung D. A drop in refrigerant R431A for replacing HFC22 in residential air-conditioners and heat pumps. 2009; 50 (7): p. 1671–5.
- [4] Aprea C, Greco A, Maiorino A. An experimental evaluation of the greenhouse effect in the substitution of R134a with  $CO_2$ . *Energy* 2012;45:753–61.
- [5] Kyoto Protocol 11; December 1997.
- [6] European Treaty 2003/87/CE.
- [7] Bisio G, Rubatto G, Schiapparelli P. Magnetic systems depending on three or two variables; thermodynamic analysis and some existing and possible applications 1999; 40 (12): p. 1267–86.
- [8] Yu BF, Gao Q, Zhang B, Meng XZ, Chen Z. Review on research of room temperature magnetic refrigeration. *Int J Refrig* 2003;26:622–36.
- [9] Gschneidner Jr KA, Pecharsky VK. Thirty years of near room temperature magnetic cooling: where we are today and future prospects. *Int J Refrig* 2008;31(6):945–61.
- [10] Pecharsky VK, Gschneidner Jr KA. Advanced magnetocaloric materials: What the future hold? *Int J Refrig* 2006;29:1239–49.
- [11] Pecharsky VK, Gschneidner Jr KA. Magnetocaloric effect associated with magneto-structural transitions. In: Planes A, Manosa L, Saxena A, editors. *Magnetism and structure in functional materials*, Springer series in materials science, vol. 79. Heidelberg: Springer; 2005. p. 199–222.
- [12] Pecharsky VK, Holm AP, Gschneidner Jr KA, Rink R. Massive magnetic-field-induced structural transformation in  $Gd_5Ge_4$  and the nature of the giant magnetocaloric effect. *Phys Rev Lett* 2003;91(19):197204.
- [13] Benford SM, Brown GV. T–S diagram for gadolinium near the Curie temperature. *J Appl Phys* 1981;52(3):2110–2.
- [14] Ponomarev BK. Apparatus for measuring the magnetocaloric effect in metal specimens in pulsed up to 8 T. *Instrum Exp Tech* 1983;26:659–62.
- [15] Ponomarev BK. Magnetic properties of gadolinium in the region of paraprocess. *J Magn Magn Mater* 1986;61:129–38.
- [16] Gopal BR, Chahine R, Bose TK. A sample translatory type insert for automated magnetocaloric effect measurements. *Rev Sci Instrum* 1997;68(4):1818–22.
- [17] Gopal BR, Chahine R, Foldeaki M, Bose TK. Non-contact thermoacoustic method to measure the magnetocaloric effect. *Rev Sci Instrum* 1995;66(1):232–8.
- [18] Foldeaki M, Schnelle W, Gmelin E, Benard P, Koszegi B, Giguere A, et al. Comparison of magnetocaloric properties from magnetic and thermal measurements. *J Appl Phys* 1997;82(1):309–16.
- [19] Nikitin SA, Talalayeva YV. Features of the magnetic behaviour and of the magnetocaloric effect in a single crystal of gadolinium. *Sov Phys JETP* 1978;47:105–9.
- [20] Ivanova TI, Levitin RZ, Nikitin SA, Talalayeva YV. Influence of the field dependence of the magnetic anisotropy constants of gadolinium on the magnetocaloric effect near the Curie point. *Phys Met Metallogr* 1981;51(4):196–9.
- [21] Kuz'min MD, Tishin AM. Magnetocaloric effect part 2: magnetocaloric effect in heavy rare earth metals and their alloys and application to magnetic refrigeration. *Cryogenics* 1993;33(9):868–82.
- [22] Dan'kov SY, Spichkin YI, Tishin AM. Magnetic entropy and phase transitions in Gd, Tb, Dy and Ho. *J Magn Magn Mater* 1996;152:208–12.
- [23] Foldeaki M, Chahine R, Bose TK. Magnetic measurements: a powerful tool in magnetic refrigerator design. *J Appl Phys* 1995;77(7):3528–37.
- [24] Dan'kov SY, Tishin AM. Experimental device for studying the magnetocaloric effect in pulse magnetic fields. *Rev Sci Instrum* 1997;68(6):2432–7.
- [25] Dan'kov SY, Tishin AM. Magnetic phase transitions and the magnetothermal properties of gadolinium. *Phys Rev B* 1998;57(6):3478–89.
- [26] Tishin AM, Gschneidner Jr KA, Pecharsky VK. Magnetocaloric effect and heat capacity in the phase transition-region. *Phys Rev B* 1999;59(1):503–11.
- [27] Griffel M, Skochdopole RE, Spedding FH. The heat capacity of gadolinium from 15 to 355 K. *Phys Rev* 1954;93(4):657–61.
- [28] Glorieux C, Thoen J, Bednarz G, White MA, Geldart DJW. Photoacoustic investigation of the temperature and magnetic field dependence of the specific heat-capacity and thermal conductivity near the Curie point of gadolinium. *Phys Rev B* 1995;52(17):12770–8.

- [29] Pecharsky VK, Moorman JO, Gschneider Jr KA. 3–350 K fast automatic small sample calorimeter. *Rev Sci Instrum* 1997;68(11):4196–207.
- [30] Pecharsky VK, Gschneider Jr KA. Magnetocaloric effect and magnetic refrigeration. *J Magn Magn Mater* 1999;200:44–56.
- [31] Gschneider Jr KA, Pecharsky VK. The influence of magnetic field on thermal properties of solids. *Mater Sci Eng* 2000;287:301–10.
- [32] Dai W, Shen BG, Li DX, Gao ZX. New magnetic refrigeration materials for temperature range from 165 K to 235 K. *J Alloys Compd* 2000;311:22–7.
- [33] Nikitin SA, Andreyenko AA, Tishin AM, Arkharov AM, Zheredev AA. Magnetocaloric effect in rare earth alloys Gd–Ho, and Gd–Er. *Phys Met Metallogr* 1985;59(2):104–8.
- [34] Wada H, Tanabe Y. Giant magnetocaloric effect of  $\text{MnAs}_{1-x}\text{Sb}_x$ . *Appl Phys Lett* 2001;79(20):3302–4.
- [35] Wada H, Morikawa T, Taniguchi K, Shibata T, Yamada A, Akishige Y. Giant magnetocaloric effect of  $\text{MnAs}_{1-x}\text{Sb}_x$  in the vicinity of first-order magnetic transition. *Physica B* 2003;328:114–6.
- [36] Brown GV. Magnetic heat pumping near room temperature. *J Appl Phys* 1976;47(8):3673–80.
- [37] Green G, Patton G, Stevens J, Humphrey J. Reciprocating of the fourth international cryocoolers conference, Easton MD; 1986.
- [38] Rowe A, Tura A. Experimental studies of near room temperature magnetic refrigeration. *Int J Refrig* 2006;29(8):1286–93.
- [39] Rowe A, Tura A. Experimental investigation of a three-material layered active magnetic regenerator. *Int J Refrig* 2006;29(8):1286–93.
- [40] Tura A, Rowe A. Progress in the characterization and optimization of a permanent magnet magnetic refrigerator. In: Proc. int. conference. of magnetic refrigeration at room temperature, IIR/IIR; 2009.
- [41] Arnold DS, Tura A, Rowe A. Experimental analysis of two-material active magnetic regenerator. *Int J Refrig* 2011;34:178–91.
- [42] Hirano N, Nagaya S, Takahashi M, Kuriyama T, Ito K, Nomura S. Development of magnetic refrigerator for room temperature application. *Adv Cryog Eng* 2002;47:1027–34.
- [43] Zimm C, Jastrab A, Sternberg A, Pecharsky V, Gschneider K, Osborne M, et al. Description and performance of a near room temperature magnetic refrigerator. *Adv Cryog Eng* 1998;43:1759–66.
- [44] Zimm C, Boeder A, Chell J, Sternberg A, Fujita S, Fujieda S, et al. Design and performance of a permanent magnet rotary refrigerator. *Int J Refrig* 2006;29(8):1302–6.
- [45] Zimm C, Boeder A, Chell J, Russek S, Sternberg A. Design and initial performance of magnetic refrigerator with a rotating permanent magnet. In: 2nd International conference on magnetic refrigeration at room temperature, Portoz, Slovenia; 2007.
- [46] Russek S, Auringer J, Boeder A, Chell J, Jacobs S, Zimm C. The performance of a rotary refrigerator with layered beds. In: Proceedings of the 4th international conference on magnetic refrigeration at room temperature, Baotou, Inner Mongolia, China; 2010. p. 339–49.
- [47] Clot P, Viallet D, Allab F, Kedous-Lebouc A, Fournier JM, Yonnet JP. A magnet based device for active magnetic regenerative refrigeration. *IEEE Trans Magn* 2003;39(5):3349–51.
- [48] Lu DW, Xu XN, Wu HB, Jin X. A permanent magnet magneto-refrigerator study on using Gd/Gd–Si–Ge/Gd–Si–Ge–Ga alloys. In: 1st International conference on magnetic refrigeration at room temperature, montreaux, Switzerland; 2005.
- [49] Okamura T, Rachi R, Hirano N, Nagaya S. Improvements of 100 W class room temperature. Portoz, Slovenia; 2007.
- [50] Yu BF, Gao Q, Zhang B, Meng XZ, Chen Z. Review on research of room temperature magnetic refrigerant. *Int J Refrig* 2003;26:622–36.
- [51] Gao Q, Yu BF, Wang CF, Zhang B, Yang DX, Zhang Y. Experimental investigation on refrigeration performance of a reciprocating active regenerator of room temperature magnetic refrigeration. *Int J Refrig* 2006;29:622–36.
- [52] Bahl CRH, Engelbrecht KL, Bjørk R, Eriksen D, Smith A, Nielsen KK, et al. Design concepts for a continuously rotating active magnetic regenerator. *Int J Refrig* 2011;34:1792–6.
- [53] Engelbrecht KL, Eriksen D, Bahl CRH, Bjørk R, Geyti J, Lozano JA, et al. Experimental results for a novel rotary active magnetic regenerator. *Int J Refrig* 2012;35:1498–505.
- [54] Balli M, Sari O, Mahmed C, Besson Ch, Bonhote Ph, Duc D, et al. A pre-industrial magnetic cooling system for room temperature application. *Appl Energy* 2012;98:556–61.
- [55] Engelbrecht KL, Nellis GF, Klein SA, Boeder AM. Modeling active magnetic regenerative refrigeration systems. In: First IIR–IIR international conference on magnetic refrigeration at room temperature montreaux, Switzerland, 27–30 September; 2005.
- [56] Engelbrecht KL, Nellis GF, Klein SA. Comparing modelling predictions to experimental data for active magnetic regenerative refrigeration systems. In: Second IIR–IIR international conference on magnetic refrigeration at room temperature Portoz, Slovenia, 11–13 April; 2007.
- [57] Dikeos J, Rowe A. Regenerator optimization through the numerical analysis of an active magnetic regenerator (AMR) refrigeration cycle. In: Weisend J et al., editors. *Advances in cryogenic engineering*, vol. 51. New York: AIP; 2006. p. 993–1000.
- [58] Pekosoy O, Rowe A. Demagnetizing effect in active magnetic regenerators. *J Magn Magn Mater* 2005;288:424–32.
- [59] Rowe A, Tura A. Active magnetic regenerator performance enhancement using passive magnetic materials. *J Magn Magn Mater* 2007;320:1357–63.
- [60] Shir F, Mavriplis C, Bennett LH, Torre Della E. Analysis of room temperature magnetic regenerative refrigeration. *Int J Refrig* 2005;28:616–27.
- [61] Allab F, Kedous-Lebouc A, Fournier JM, Yonnet JP. Numerical modelling for active magnetic regenerative refrigeration. *IEEE Trans Magn* 2005;41(10):3757–9.
- [62] Boučekara H, Kedous-Lebouc A, Dupuis C, Allab F. Prediction et optimisation of geometrical properties of the refrigerant bed in an AMRR cycle. *Int J Refrig* 2008;31(7):1224–30.
- [63] Petersen TF, Pryds N, Smith A, Hattel J, Schmidt H, Knudsen Høgaard H. Two-dimensional mathematical model of a reciprocating room-temperature active magnetic regenerator. *Int J Refrig* 2008;31:432–43.
- [64] Nielsen KK, Bahl CRH, Smith A, Bjørk R, Pryds N, Hattel J. Detailed numerical modelling of a linear parallel-plate active magnetic regenerator. *Int J Refrig* 2009;32:1478–86.
- [65] Bouchard J, Nesreddine H, Galanis N. Model of a porous regenerator used for magnetic refrigeration at room temperature. *Int J Heat Mass Transfer* 2009;52:1223–9.
- [66] Petersen TF, Engelbrecht K, Bahl C, Elmegeard B, Pryds N, Smith A. Comparison between a 1D and a 2D numerical model of an active magnetic regenerative refrigerator. *J Phys D: Appl Phys* 2008;41:105002–10.
- [67] Barclay JA. The theory of an active magnetic regenerative refrigerator. NASA STI/Recon Technical Report N 83, 34087; 1982.
- [68] Aprea C, Greco A, Maiorino A. A numerical analysis of an active magnetic regenerative cascade system. In: 3rd International conference on magnetic refrigeration at room temperature, IIR conference, Des Moines, United States, May 11–15; 2009.
- [69] Aprea C, Greco A, Maiorino A. A numerical analysis of an active magnetic regenerative cascade system. *Int J Energy Res* 2011;35:177–88.
- [70] Aprea C, Greco A, Maiorino A. Modelling an active magnetic refrigeration system: a comparison with different models of incompressible flow through a packed bed. *Appl Therm Eng* 2012;36:296–306.
- [71] Aprea C, Greco A, Maiorino A. A numerical analysis of an active magnetic regenerative refrigerant system with a multi-layer regenerator. *Energy Convers Manage* 2011;52:97–107.
- [72] Bozorth RM. Energy, specific heat, and magnetocaloric effect, ferromagnetism. New Jersey: D. Van Nostrand Company; 1956. pp. 729–744.
- [73] Shir F, Della Torre E, Bennett LH, Mavriplis C, Shull RH. Modelling of magnetization and demagnetization in magnetic regenerative refrigeration. *IEEE Trans Magn* 2004;40:2098–100.
- [74] Allab F, Kedous-Lebouc A, Yonnet JP, Fournier JM. A magnetic field source system for magnetic refrigeration and its interaction with magnetic material. *Int J Refrig* 2006;29(8):1340–7.
- [75] Tishin AM, Spichkin YI. The magnetocaloric effect and its applications. Bristol and Philadelphia: Institute of Physics Publishing; 2003. p. 13–4.
- [76] Bingfeng Y, Zhang Y, Qiang G, Dexi Y. Research on performance of regenerative room temperature magnetic refrigeration cycle. *Int J Refrig* 2006;29:1348–57.
- [77] Bouvier M, Lethuillier P, Schmitt D. Specific heat in some gadolinium compounds. I. Experimental. *Phys Rev B* 1991;43(16):13137–44.
- [78] Blanco JA, Gignoux D, Schmitt D. Specific heat in some gadolinium compounds. II. Theoretical model. *Phys Rev B* 1991;43(16):13145–51.
- [79] Aprea C, Maiorino A. A flexible numerical model to study an active magnetic refrigerator for near room temperature applications. *Appl Energy* 2010;87:2690–8.
- [80] Peksoy O, Rowe A. Demagnetization effects in active magnetic regenerators. *J Magn Magn Mater* 2005;288:424–32.
- [81] Yu B, Gao Q, Yang D, Zhang Y. Research on performance of regenerative room temperature magnetic refrigeration cycle. In: Refrigeration science and technology proceedings of the international conference on magnetic refrigeration at room temperature, Montreaux; 2005. p. 9–68.
- [82] Ramji RR, Narayana Murty JVSS. Magnetic contribution to the specific heats of gadolinium, dysprosium and erbium. *J Low Temp Phys* 1978;33:413–8.
- [83] Smaili A, Chahine R. Thermodynamic investigations on optimum active magnetic regenerators. *Cryogenic* 1998;38:247–52.
- [84] Balli M, Allab F, Dupuis C, Fruchart D, Gignoux D, Kedous-Lebouc A, Fournier JM, Yonnet JP. Analysis and modelling of magnetocaloric effect near magnetic phase transition temperature. In: Second IIR–IIR international conference on magnetic refrigeration at room temperature, Portozm Slovenia, 11–13 April; 2007.
- [85] Balli M, Fruchart D, Gignoux D, Miraglia S, Hlil EK, Wolfers P. Modelling of the magnetocaloric effect in  $\text{Gd}_{1-x}\text{Tb}_x$  and  $\text{MnAs}$  compounds. *J Magn Magn Mater* 2007;316:558–61.
- [86] Balli M, Fruchart D, Gignoux D, Miraglia S, Hlil EK, Miraglia S, et al.  $\text{Gd}_{1-x}\text{Tb}_x$  alloys for ericsson-like magnetic refrigeration cycles. *J Alloy Compd* 2007;442:129–31.
- [87] Moore JD, Perkins GK, Bugoslavsky Y, Chattopadhyay MK, Roy SB, Chaddah P, et al. Reducing the operational magnetic field in the prototype magnetocaloric system  $\text{Gd}_5\text{Si}_2\text{Ge}_2$  by approaching the single cluster size limit. *Appl Phys Lett* 2006;88:072501.
- [88] Pecharsky VK, Gschneider Jr KA. Effect of alloying on the giant magnetocaloric effect of  $\text{Gd}_5\text{Si}_2\text{Ge}_2$ . *J Magn Magn Mater* 1997;167:179–84.
- [89] Pecharsky VK, Gschneider Jr KA. Giant magnetocaloric effect in  $\text{Gd}_5\text{Si}_2\text{Ge}_2$ . *Phys Rev Lett* 1997;78(23):4494–7.
- [90] Pecharsky VK, Gschneider Jr KA. Tunable magnetic regenerator alloys with a giant magnetocaloric effect for magnetic refrigeration from 20 to 290 K. *Appl Phys Lett* 1997;70(24):3299–301.

- [91] Pecharsky VK, Samolyuk GD, Antropov VP, Pecharsky AO, Gschneidner Jr KA. The effect of varying the crystal structure on the magnetism, electronic structure and thermodynamics in the  $Gd_5Si_xGe_{4-x}$  alloys for  $1.4 \leq x \leq 2.2$ . *J Magn Mater* 2003;267:60–8.
- [92] Pecharsky VK, Samolyuk GD, Antropov VP, Pecharsky AO, Gschneidner Jr KA. The effect of varying the crystal structure and thermodynamics in the  $Gd_5Si_xGe_{4-x}$  system near  $x = 0.5$ . *J Solid State Chem* 2003;171:57–68.
- [93] Gschneidner Jr KA, Pecharsky VK, Tsokol AO. Recent developments in magnetocaloric materials. *Rep Prog Phys* 2005;68:1479–539.
- [94] Bean CP, Rodbell DS. *Phys Rev* 1961;126:104.
- [95] Rodbell DS. *Phys Rev Lett* 1961;7:1.
- [96] von Ranke PJ, Oliveira NA, Gama S. Theoretical investigation on giant magnetocaloric effect in  $MnAs_{1-x}Sb_x$ . *Phys Lett A* 2004;320:302–6.
- [97] Amiri A, Vafai K. Transient analysis of incompressible flow through a packed bed. *Int J Heat Mass Transfer* 1998;41:4259–79.
- [98] Pei-Xue J, Ze-pei R, Bu-Xuan W. Numerical simulation of forced convection heat transfer in porous plate channels using thermal equilibrium and nonthermal equilibrium models. *Numer Heat Transfer Part A* 1999;35:99–113.
- [99] Klein H, Eigenberger G. Approximate solutions for metallic regenerative heat exchangers. *Int J Heat Mass Transfer* 2001;35:53–63.
- [100] Nellis GF, Klein SA. Regenerative heat exchangers with significant entrained fluid heat capacity. *Int J Heat Mass Transfer* 2006;49:329–40.
- [101] Shen Chien-Ming, Worek WM. The effect of wall conduction on the performance of regenerative heat exchangers. *Energy* 1992;17(12): 1199–213.
- [102] Vafai K, Sözen M. Analysis of energy and momentum transport for fluid flow through a porous bed. *J Heat Transfer* 1990;112:690–9.
- [103] Amiri A, Vafai K. Analysis of dispersion effects and non-thermal equilibrium, non-Darcian, variable porosity incompressible flow through porous media. vol. 37; 1994. p. 939–54.
- [104] Nakayama A, Kuwahara F, Sano Y. Concept of equivalent diameter for heat and fluid flow in porous media. *AIChE J* 2007;732–6.
- [105] Wakao N, Kaguei S, Funazkri T. Effect of fluid dispersion coefficients on particle-to-fluid heat transfer coefficients in packed beds. *Chem Eng Sci* 1979;34:325–36.
- [106] Wakao N, Kaguei S. Heat and mass transfer in packed beds. New York: Gordon and Breach; 1982.
- [107] Hunt ML, Tien CL. Non-darcian convection in cylindrical packed beds. *J Heat Transfer* 1988;110:378–84.
- [108] Feng Y, Boming Yu, Mingqing Z, Duanming Z. A generalized model for the effective thermal conductivity of porous media based on self-similarity. *J Phys D Appl Phys* 2004;37:3030–40.
- [109] Kaviany M. Principles of heat transfer in porous media. New York, NY: Springer; 1995. p. 33, 46–7, 130, 228–229.
- [110] Rice K. DOE/ORNL heat pump model, mark VI version; 2006.
- [111] Gschneidner Jr KA, Mudryk Y, Pecharsky VK. On the nature of the magnetocaloric effect of the first order magnetostructural transition. *Scr Mater* 2012;67:572–877.